Estimation of Atmospheric Profiles From Hyperspectral Infrared IASI Sensor

Hua Wu, Li Ni, Ning Wang, Yonggang Qian, Bo-Hui Tang, and Zhao-Liang Li

***Abstract*—A physics-based regression algorithm was developed and applied to the Infrared Atmospheric Sounding Interferometer (IASI) observations to estimate atmospheric temperature and humidity profiles. The proposed algorithm utilized three steps to solve the ill-posed problems and to stabilize the solution in a fast speed regression manner: 1) a set of optimal channels was selected to decrease the effect of forward model errors or uncertainties of trace gases; 2) the principal component analysis technique was used to reduce the number of unknowns; 3) a ridge regression procedure was introduced to improve the ill-conditioned problem and to lessen the influence of correlation. To determine the optimal coefficients of the algorithm, a simulated dataset was generated with the spectral emissivities and atmospheric profiles fully covering all the possible situations for clear sky conditions. Then, the accuracy of the algorithm was evaluated against with both simulated and actual IASI data. The root mean squared error (RMSE) of atmospheric temperature profile for the simulated data is about 1.5 K in troposphere and stratosphere and is close to 4 K near the surface with no biases. The RMSE of atmospheric humidity profile for the simulated data is about 0.001–0.003 g/g at low altitude. Although the retrieval accuracy for the actual IASI data is not as good as those for the simulated data, the vertical distribution of atmospheric profiles can be well captured. Those results showed that the proposed algorithm is promising when the profile bias errors could be removed.**

***Index Terms*—Atmospheric humidity profile, atmospheric temperature profile, hyperspectral thermal infrared, IASI, inverse problems, remote sensing.**

I. Introduction

THE atmospheric temperature and humidity profiles are of great importance in climate research, and weather prediction among others, and will clearly continue to be important for the foreseeable future [1]. How to accurately retrieve atmospheric profiles from space has attracted more attentions in recent years. However, the accuracy of retrieval is generally limited due to the coupling of land surface and atmosphere [2]–[6]. This problem makes the accurate retrieval of atmospheric profiles need land surface temperature and emissivity as *a priori* knowledge, and vice versa [7], [8]. Furthermore, the low vertical resolution of traditional multispectral sensors degrades the retrieval accuracy because each channel of these sensors receives energy emitted from a thick layer of the atmosphere. In addition, the discrepancy between the scales of remote sensed observations and those of radiosonde measurements brings troubles for the validations of the retrieved atmospheric profiles [9].

Recently, the hyperspectral infrared sensors, such as Atmospheric InfraRed Sounder (AIRS), Infrared Atmospheric Sounding Interferometer (IASI), and Cross-track Infrared Sounder (CrIS), have been equipped on polar orbiting platforms. Each of these sensors has thousands of channels for a single field of view. It brings hope that land surface temperature/emissivity and atmospheric profiles can be accurately retrieved with an improved vertical resolution from these sensors [10]. However, the retrieval in fact is still an ill-posed problem [2]. The number of unknowns is always larger than that of measurements. The key is to reduce the number of unknowns or increase the number of equations to make the problem deterministic. To date, various attempts from empirical to physical methods to extract the atmospheric profiles from space have been proposed [1], [2], [7], [8], [11]–[13]. The computational expense of physically based methods has generally made empirically based methods attractive when facing mass hyperspectral data [2]. However, advances in technology will allow computationally intensive physical methods to be implemented and attract more focus in the near future.

To estimate the atmospheric profiles as accurately as possible and provide first-guesses for a subsequent study of physical method to synthetically retrieve both land surface and atmospheric parameters, a physics-based regression algorithm for hyperspectral infrared IASI data was proposed to retrieve atmospheric profiles under clear sky conditions by using a set of optimal channels and by introducing principal components and a ridge regression. Section II is devoted to describe the theory basis for atmospheric profiles retrieval from space and to give the solution of regression coefficients in eigenvector domain. Section III will describes the data used for this study. Section IV gives some evaluation results against with both the simulated data and the actual *in situ* radiosonde data. Finally, conclusions are summarized in the last section.

Manuscript received September 30, 2012; revised December 08, 2012; accepted March 11, 2013. Date of publication June 03, 2013; date of current version June 17, 2013. This work was supported in part by the National Natural Science Foundation of China under Grants 41101332, 41231170, and 41071231, and by the National High Technology Research and Development Program of China under Grant 2012AA121103. *(Corresponding author: Z.-L. Li.)*

H. Wu and B.-H. Tang are with the State Key Laboratory of Resources and Environment Information System (LREIS), Institute of Geographic Science and Nature Resources Research (IGSNRR), Chinese Academy of Sciences (CAS), Beijing 100101, China (e-mail: wuhua@igsnrr.ac.cn; tangbh@igsnrr.ac.cn).

L. Ni is with the Key Laboratory of Digital Earth Science, Center for Earth Observation and Digital Earth, Chinese Academy of Sciences, Beijing 100094, China (e-mail: lni@ceode.ac.cn).

N. Wang and Y. Qian are with the Academy of Opto-Electronics, Chinese Academy of Sciences, Beijing, 100094, China (e-mail: wangning@aoe.ac.cn; qianyg@aoe.ac.cn).

Z.-L. Li is with the Key Laboratory of Agri-informatics, Ministry of Agriculture/Institute of Agricultural Resources and Regional Planning, Chinese Academy of Agricultural Sciences, Beijing 100081, China, and also with ICube, UdS, CNRS, 67412 Illkirch, France (e-mail: lizhaoliang@caas.cn).

Color versions of one or more of the figures in this paper are available online at http://ieeexplore.ieee.org.

Digital Object Identifier 10.1109/JSTARS.2013.2258138

II. Methodology

A. Radiative Transfer Equation

An infrared sensor onboard a satellite viewing Earth's surface measures the radiance emitted from Earth and its atmosphere along the line of sight. Assuming a cloud-free atmosphere under local thermodynamic equilibrium and neglecting the atmospheric scattering effects, the radiative transfer equation (RTE) in the infrared region can be written as:

$$\begin{aligned} R(v,\theta) = {} & \varepsilon(v,\theta)B(v,T_s)\tau(v,\theta,p_s) \\ & - \int_0^{p_s} B(v,T_p)\frac{\partial \tau(v,\theta,p)}{\partial p}dp \\ & + (1-\varepsilon(v,\theta))\int_0^{p_s} B(v,T_p)\frac{\partial \tau^*(v,\theta,p)}{\partial p}dp + R' , \end{aligned} \tag{1}$$

where R is the spectral radiance measured at the top of the atmosphere (TOA) with wavenumber v and viewing zenith angle θ. For simplicity, the wavenumber and viewing zenith angle are ignored in the following expressions. ε is the effective land surface emissivity. B is the Planck function of the temperature. T_s and T_p are land surface and atmospheric temperature, respectively. τ is the transmittance from the pressure level p to the TOA along the viewing angle. $\tau^*(v,\theta,p)$ is the reflected transmittance from surface p_s to the pressure level p. The subscript s denotes surface values. R' is the reflected solar radiation, which can be ignored in the longwave infrared window region. The first term of (1) at the right hand represents surface emission to space. The second term is the upwelling radiance contributed from atmosphere to space. The third term denotes the atmospheric downwelling emissive radiance reflected by the surface to space.

Equation (1) may be approximated in the numerical perturbation form by using the first order variation [2]:

$$\begin{aligned} \delta T_B = {} & W_{T_s}\delta T_s + W_\varepsilon \delta\varepsilon \\ & + \int_0^{p_s} W_T \delta T_p dp + \int_0^{p_s} W_{q_w}\delta \ln q_w dp , \end{aligned} \tag{2}$$

where the perturbation δ is with respect to an *a priori* mean condition. T_B is a brightness temperature vector. W_{Ts}, W_ε, W_{Tp}, and W_{qw} are the weighting functions of land surface temperature (T_s), surface emissivity (ε), atmospheric temperature (T_p), and water vapor (qw), respectively. Consequently, (1) can be linearized to perturbations of T_s, ε, T_p, and qw by introducing a background mean condition.

Equation (2) can be simplified in its matrix form as:

$$\delta T_B = K\delta x , \tag{3}$$

where the weighting function matrices K is the linear or tangent model of the forward radiative transfer model and can be calculated by a differential scheme or analytical method [2], [14]. The perturbation matrices δx are the perturbed unknowns related to the land surface and atmospheric profiles.

B. Solution in the Eigenvector Domain

Obviously, (3) still presents an ill-posed problem. The number of unknowns is larger than that of equations. To reduce the uncertainties in the solution and take advantage of spectral correlations, the atmospheric temperature and humidity profiles as well as the emissivity spectra can be represented by their eigenvectors, making only a few unknowns, i.e., coefficients of eigenvectors, need to be solved in the retrieval. Therefore, it greatly reduces the number of unknowns to the same order as that of equations. In the eigenvector domain the perturbation matrix can be written as:

$$\delta x = \sum_{i=1}^{M} f_i v_i = Vf , \tag{4}$$

where v_i is the ith eigenvector, f_i is the associated coefficient, and M is the number of eigenvectors used. V and f are the corresponding eigenvector matrix and coefficient vector. In the eigenvector domain, (3) becomes:

$$\delta T_B = K\delta x = KVf = \tilde{K}f. \tag{5}$$

Because of the high correlation within the equations, the observation errors may have a great effect on the retrieval accuracy. To reduce this effect, a ridge regression is introduced to stabilize the solution and to obtain reliable regression coefficients at the expense of losing small accuracies and biasing estimate [15]. Therefore, the solution of regression coefficients in (5) can be given by:

$$f = (\tilde{K}^T\tilde{K} + rI)^{-1}\tilde{K}^T\delta T_B , \tag{6}$$

where r is the ridge parameter and I is the identity matrix. Small positive values of r will improve the conditioning of the problem. The coefficients can be used to establish the relationship between the perturbation of brightness temperature and that of the unknown parameters of interest with respect to the background mean condition. Once these coefficients are known, the parameters of interest departure from the *a priori* mean condition can be estimated from (4).

C. Selection of a Subset of Channels

Because of the huge volume of data, the forward model errors, as well as the uncertainties about trace gases, a channel selection procedure should be implemented to make the total loss of information be a minimum and the retrieval accuracy be less affected by the errors or uncertainties. Collard [16] advised that the shortwave channels ($\lambda <= 5\ \mu\mathrm{m}$) can be affected by sunlight and should not be chosen in preference to longwave channels that can provide similar information. In addition, channels should be avoided if they are sensitive to elements not in the radiative transfer model, or are sensitive to variable species whose variability is not considered in the background or in the retrieval; or have known radiative transfer weaknesses [16]. In the end, 226 channels out of 8461 spectral channels of IASI as shown by Fig. 1 for atmospheric profile retrieval were optimally selected as that proposed by Collard [16] from 650 cm^{-1} to 1600 cm^{-1}.

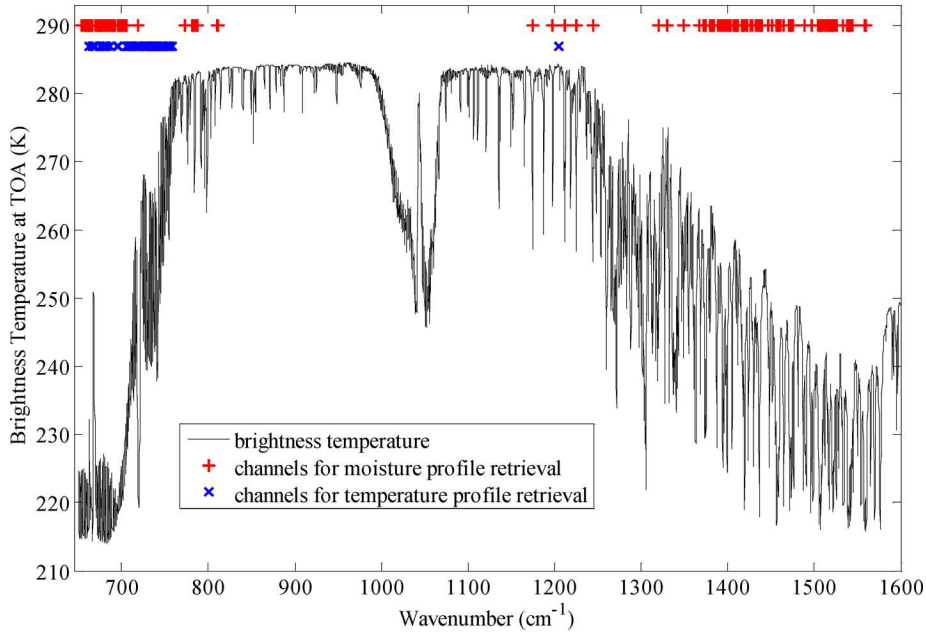

Fig. 1. The locations of selected channels for the atmospheric profile retrieval.

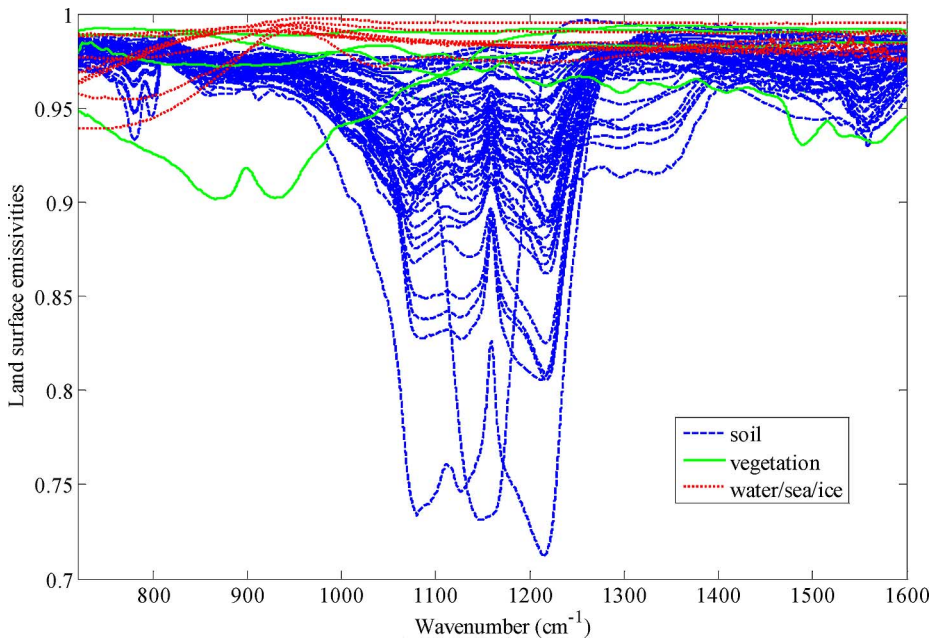

Fig. 2. The spectral variation of the selected land surface emissivities of soil, vegetation, and water/sea/ice.

III. Data

A. The Database of Spectral Emissivities and Atmospheric Profiles

To simulate the radiances at TOA representing a worldwide set of atmospheric situations and land surface types and to determine the regression coefficients, the Advanced Spaceborne Thermal Emission Reflection Radiometer (ASTER) spectral library and thermodynamic initial guess retrieval (TIGR) database were used.

The ASTER spectral library includes data from three other spectral libraries: the Johns Hopkins University (JHU) Spectral Library, the Jet Propulsion Laboratory (JPL) Spectral Library, and the United States Geological Survey (USGS) Spectral Library. It is a compilation of more than 2300 spectra of materials, including minerals, rocks, soils, vegetation, lunar and manmade materials, covering the wavelength range 0.4–15.4 μm [17]. The spectra of main materials (soils, vegetation, water, and snow/ice) of the terrestrial ecosystem, including 52 soil types, 4 vegetation types, 9 water/snow/ice types, were chosen to develop the algorithm in this study in Fig. 2.

The TIGR atmospheric profiles constructed by the Laboratoire de Meteorologie Dynamique (LMD) represent a worldwide set of atmospheric situations from polar to tropical atmosphere. TIGR contains 2311 atmospheric temperature, humidity and ozone mixing ratio profiles selected from a collec-

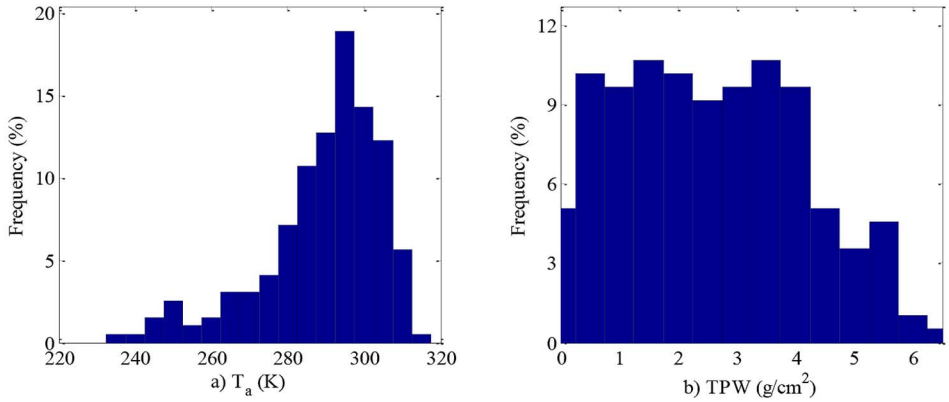

Fig. 3. The histogram of selected atmospheric quantities. (a) the bottom atmospheric temperature, (b) the total precipitable water of profiles.

tion of more than 150,000 radiosonde measurements around the world with total precipitable water (TPW) ranging from 0.1 to 8.0 $\mathrm{g/cm^2}$. TIGR supplies these profiles in 40 pressure levels from 0.05 to 1013 hPa. These profiles are grouped into five airmass types, including 872 profiles in tropical airmass, 388 in mid-latitude-1, 354 in mid-latitude-2, 104 in polar-1 and 593 in polar-2. Since the final objective is to synthetically retrieve the land surface and the atmospheric parameters in the near future, only atmospheric profiles in clear sky are taken into account here. Consequently, a profile selection procedure was performed to choose the cloud-free atmospheric situations. In this procedure, the profiles with relative humidity at any layer greater than 90% or at two consecutive layers greater than 85% were considered to be cloudy [18]. Moreover, a subset of the remained profiles was further elaborately selected to insure that there was a nearly uniform probability distribution for TPW. At last, 196 atmospheric profiles, with the bottom atmospheric temperature (T_a) varying between 220 K and 320 K and TPW nearly equally distributed between 0–6.5 $\mathrm{g/cm^2}$ were extracted from TIGR in Fig. 3.

B. Hyperspectral Infrared IASI Data and Corresponding Radiosonde Observations

The hyperspectral infrared IASI data are used to evaluate the proposed method in this paper. IASI is one of the key payloads on MetOp-A which was successfully on orbit on October 19th, 2006. IASI is a kind of Fourier transform spectrometer with 8461 spectral channels covering a spectral range from 645 to 2760 $\mathrm{cm^{-1}}$ (3.6–15.5 $\mu\mathrm{m}$). The spectral resolution is 0.5 $\mathrm{cm^{-1}}$ (full width at half maximum) after apodisation. The spectral sampling interval is 0.25 $\mathrm{cm^{-1}}$. IASI is an across track scanning system with scan range of $\pm 48^\circ 20'$, symmetrically with respect to the nadir direction. Each scan line contains 30 scan positions towards the Earth and two calibration views. At each scan position, the effective field of view (EFOV) consists of a 2×2 matrix of instantaneous fields of view (IFOV) with a diameter of 14.65 mrad, corresponding to a ground spatial resolution of about 12 km at nadir with a satellite altitude of 819 km. A series of IASI data can be found and downloaded from the European Organization for the Exploitation of Meteorological Satellites (EUMETSAT) net site (http://www.eumetsat.int). In this work, the level 1C products with the observed radiances were used in the evaluation of the proposed regression algorithm. The IASI Level 1C products provide us the geo-located, calibrated, resampled and apodised radiance spectra.

Radiosondes carried by balloons can be used to measure and simultaneously transmit recorded data, which includes pressure, temperatures and humidity. Balloons generally can reach altitudes as high as 30 km prior to bursting, about 90 minutes after launch. Horizontal distances traveled by the balloon may exceed 200 km, but this varies significantly depending on the nature of winds in the upper atmosphere. Radiosonde observations usually are taken twice daily at 00:00 hours and 12:00 hours at Universal Time Coordinated (UTC). Atmospheric data from the radiosonde are interpreted at the launching station and have entered into a worldwide communications network. Current and old radiosonde observations from nearly 686 stations around the world can be found at the University of Wyoming website (http://weather.uwyo.edu/upperair/sounding.html).

Because the evaluation of the proposed method requires the time and location matching pairs of IASI data and radiosonde observations, a two-line element set (TLE) of MetOp-A, which describes the orbits of Earth-orbiting satellites, was used to track the location of the nadir of satellite, and to match the radiosonde data. Taking into account the fact that there are often no corresponding radiosonde data at UTC 12:00 for unclear reasons, the UTC 00:00 are set as the reference time to search the corresponding pairs of IASI data and radiosonde observations. Fig. 4 showed the distribution of radiosonde stations around world and the traces of the nadir of IASI at UTC 00:00 in 2009 and 2010, respectively.

It is obvious that most matching places are fallen into the ocean. To fully evaluate the proposed algorithm in the land, Australia was selected as the study area as shown in Fig. 5.

Finally, 62 scenes of IASI data in 2009 and 51 scenes in 2010, which fly overpass the radiosonde stations at UTC 00:00, were filter out according to the strict matching rule of data acquisition-time. Excluding quasi-cloud-contaminated scenes, 22 scenes in 2009 and 18 scenes in 2010 were selected with simultaneous atmospheric profiles from the radiosonde stations in our evaluation study. The acquisition dates of selected IASI data were uniformly distributed from January to December in 2009

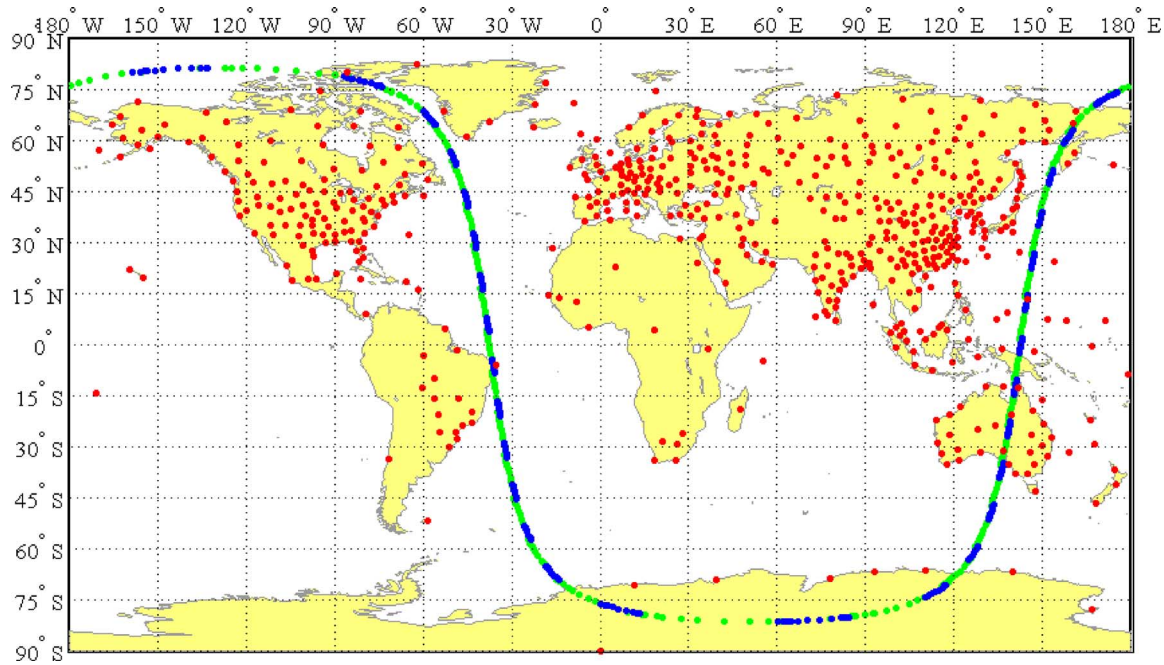

Fig. 4. Illustration of the distribution of radiosonde stations around world and the traces of the nadir of IASI at UTC 00:00 in 2009 and 2010. The red circles are the locations of radiosonde stations, while the blue and green circles are the traces in 2009 and 2010, respectively.

and 2010. The traces for the nadirs of those IASI data were also shown in Fig. 5.

IV. Results

A. Determination of Regression Coefficients

To determine the regression coefficients from (6), the use of simulated data rather than actual measurements is more advisable due to the difficulty in collecting the synchronous measurements. Taking this reason into account, the selected land surface emissivities and atmospheric profiles as well as the hyperspectral atmospheric radiative transfer model 4A/OP (Operational Release for Automatized Atmospheric Absorption Atlas) [19] were used to simulate the radiance at TOA for IASI. The simulated data were then used to get the regression coefficients, and to evaluate the algorithm accuracies. The spectral range of the simulation was spanning from 650 to 1600 cm^{-1}, with spectral resolution about 0.5 cm^{-1} and sampling interval about 0.25 cm^{-1} similar to the configuration of IASI. The noise equivalent temperature differences ($\text{NE}\Delta\text{T}$) of the IASI were adopted from that of Aires [20]. To make the simulation more representatives, the reasonable variations of LST were varied in a wide range according to T_a of the atmospheric profiles used. That is, LST varied from $T_a - 5$ K to $T_a + 15$ K in steps of 5 K for $T_a - 290$ K and from $T_a - 5$ K to $T_a + 5$ K in steps of 5 K for $T_a < 290$ K [21]. Taking into account the angular dependence of TOA radiance, nine different viewing zenith angles (VZAs) (0°, 24.62°, 33.56°, 39.72°, 44.42°, 48.19°, 51.32°, 56.25°, 60°) were used in simulations. In total, 531700 different situations were obtained for each VZA. Finally, the regression coefficients f were obtained directly through (6). Due to the small intervals of VZAs used in simulations, the regression coefficients for other VZAs were linearly interpolated in function of the secant VZA.

B. Evaluation With the Simulated IASI Data

The final retrieved results with the simulated IASI data, which are the same as those in determination of regression coefficients, were shown in the following figures.

Fig. 6 shows the bias and the standard deviation of the retrieved atmospheric profiles for the simulated IASI data with 531700 different situations at VZA 0°. Obviously, both atmospheric temperature and humidity profiles at different altitude are estimated with no biases. The standard deviations are larger at the bottom of atmosphere and they decrease with increasing altitude until reaching to a fix value at certain pressure.

Fig. 7 shows the root mean square errors (RMSEs) of the retrieved atmospheric profiles for the simulated IASI data. From this figure, we can see that the RMSE of temperature profile is about 1.5 K in troposphere and stratosphere and is close to 4 K near the surface. It can also be found that the errors of temperature profile kept nearly invariable along with the altitude except for that near the surface. The probable reasons are: 1) the accuracies at the bottom of atmosphere may be degraded by the couple of land-atmosphere; 2) the selected channels are more sensitive to the atmosphere in the middle and upper of troposphere, which means those channels can well detect the temperature profiles at different altitudes in a vertical atmospheric column especially beyond 700 hPa. Meanwhile, the accuracies of the proposed algorithm could be improved by introducing more atmospheric windows or combining with the Advanced Microwave Sounding Unit (AMSU) observation to increase the channels in which the peak of the weighting functions locates near the surface. The RMSE of atmospheric humidity profile is about 0.001–0.003 g/g at low altitude. Those errors decrease greatly along with the altitude beyond the troposphere.

The retrieval results at other VZAs will not be shown here for their similar performances.

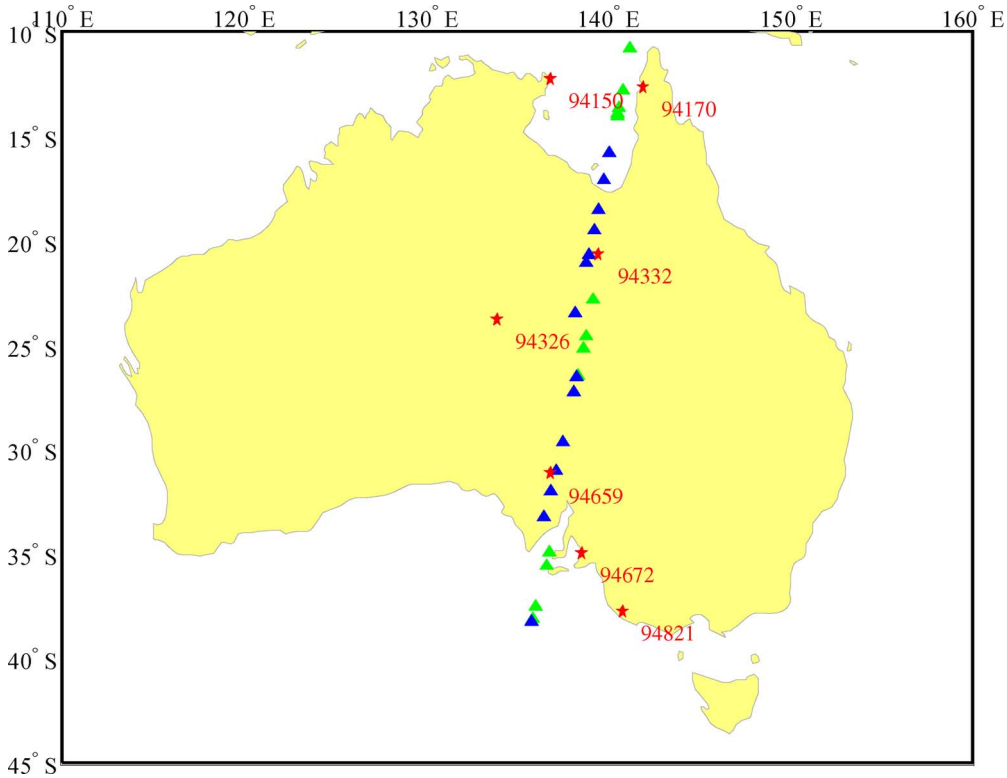

Fig. 5. Illustration of selected study area of Australia. The red pentacles are the locations of the selected radiosonde stations, and the texts at the right bottom of pentacles show the station IDs. The green and blue triangles (some are overlapping) are the the traces of the nadir of the selected IASI data in 2009 and 2010, respectively.

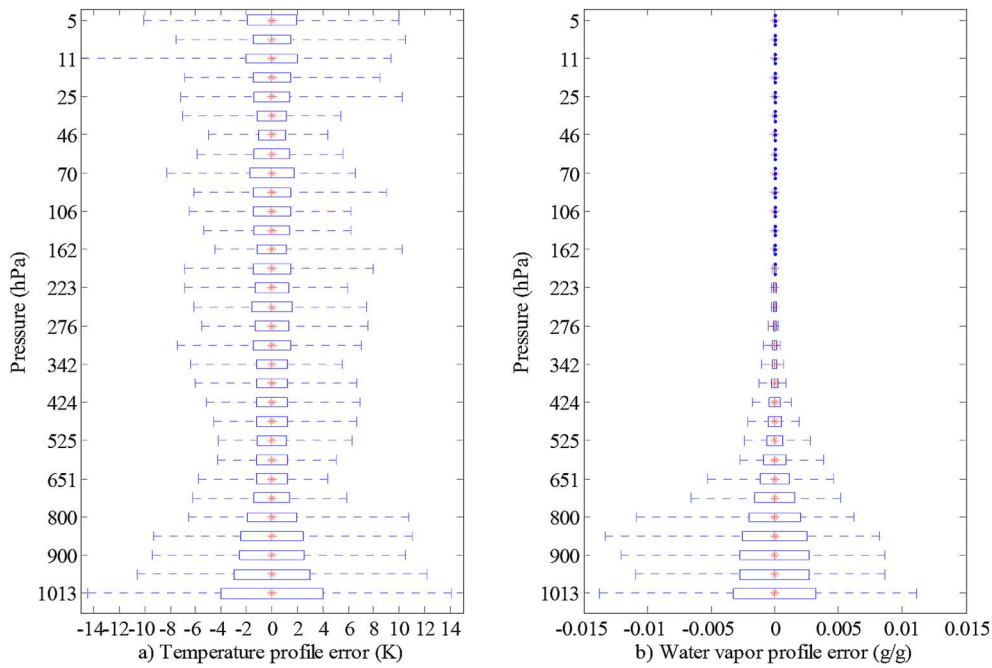

Fig. 6. The bias and the standard deviation of the retrieved atmospheric profiles for the simulated IASI data with 531700 different situations at VZA 0°. The red asterisks indicate the biases and the half length of horizontal bars is equal to the standard deviation. (a) for temperature profile; (b) for humidity profile.

C. Evaluation With the Actual IASI Data

In this work, the proposed algorithm was also carried out with the selected scenes of IASI data. The retrieved atmospheric profiles were compared with the *in situ* radiosonde observations.

To demonstrate the performance of the algorithm, two cases out of eighteen scenes, one for summer and the other for winter, are selected and shown in Fig. 8. Both the retrieved temperature and water vapor mixing ratio profiles have good agreements with the radiosonde measurements especially at the middle and

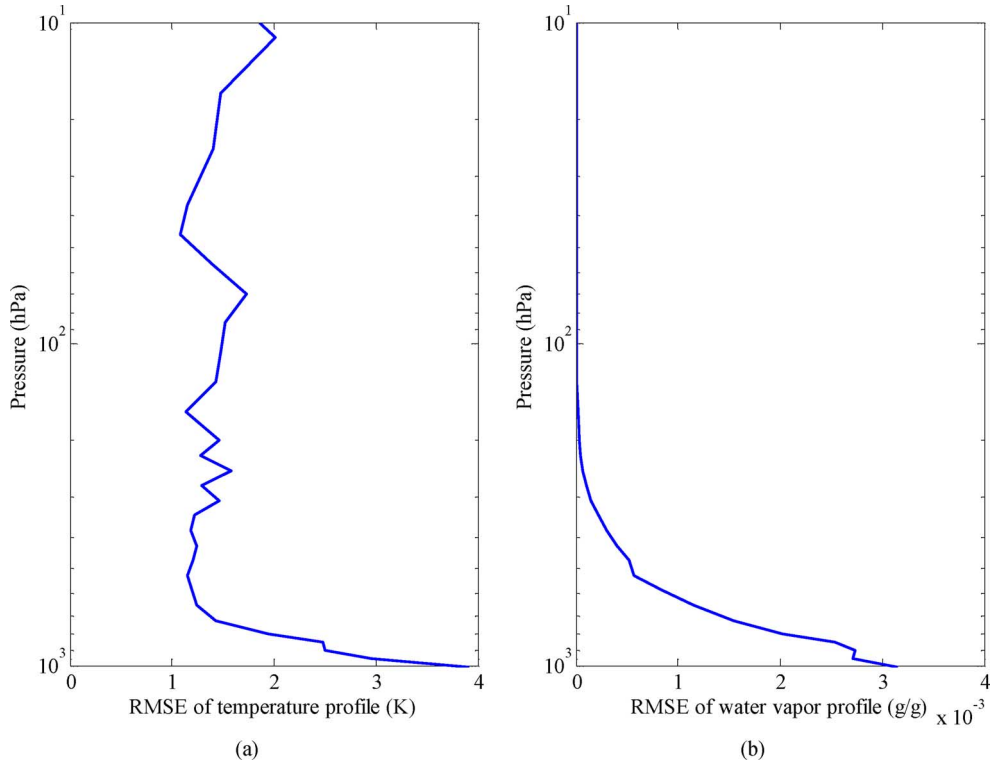

Fig. 7. The RMSEs of the retrieved atmospheric profiles for the simulated IASI data with 531700 different situations at VZA 0°. (a) For temperature profile; (b) for humidity profile.

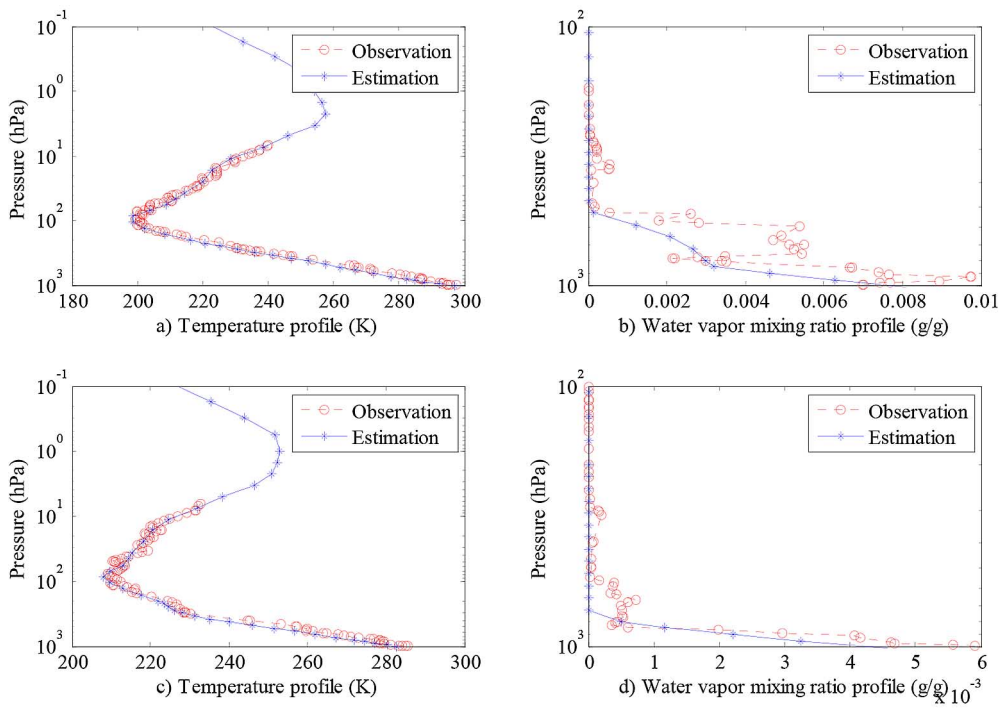

Fig. 8. Comparison of the atmospheric profiles retrieved from actual IASI data using the proposed algorithm with those measured by radiosonde for two days (one for summer and the other for winter). The red circles (dashed) represent the radiosonde observations while the blue asterisks (solid) represent the retrieved profiles. The ordinates are the atmospheric pressure in logarithmic scale. (a) and (b) are for temperature and water vapor mixing ratio profile against with observations of radiosonde station 94659 at UTC 00:00 on February 24th, 2010; (c) and (d) are for temperature and water vapor mixing ratio profile against with observation of radiosonde station 94659 at UTC 00:00 on August 17th, 2010.

upper troposphere. The vertical distribution of atmospheric profiles can be well captured by the proposed algorithm.

To fully evaluate the proposed algorithm, the statistics for the eighteen actual IASI data in 2010 are shown in Fig. 9.

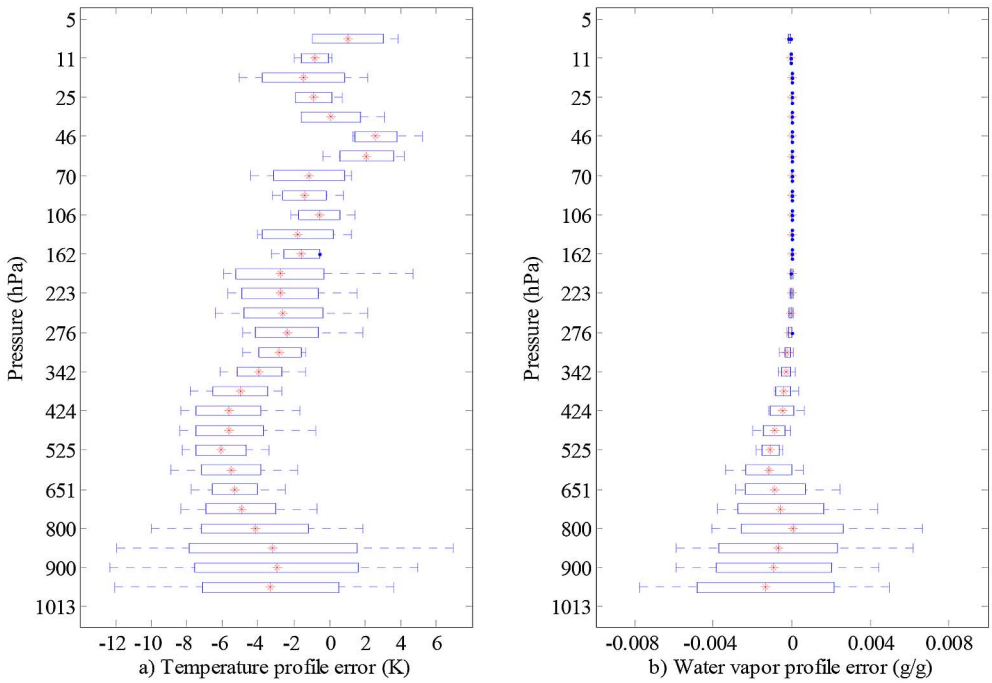

Fig. 9. The bias and the standard deviation of the retrieved atmospheric profiles for the actual IASI data in 2010. The red asterisks indicate the biases and the half length of horizontal bars is equal to the standard deviation. (a) for temperature profile; (b) for humidity profile.

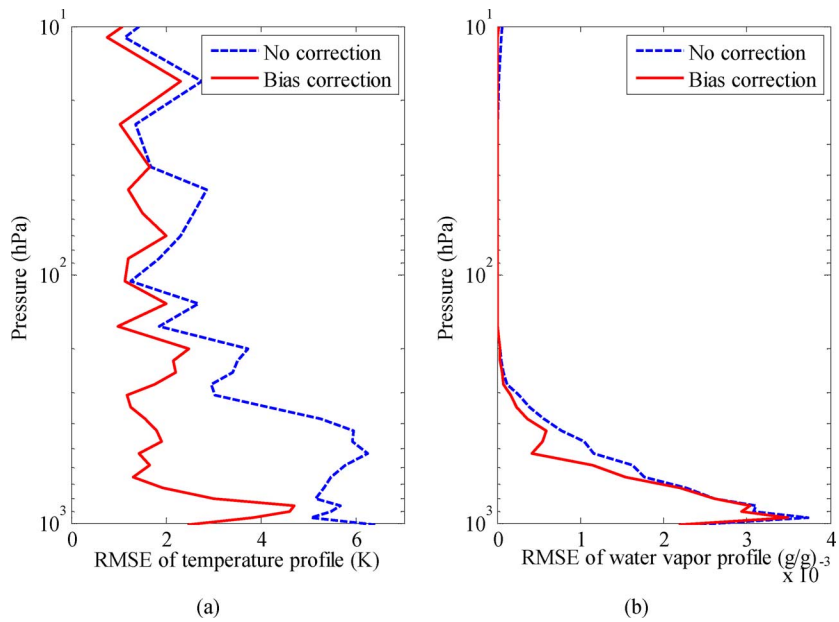

Fig. 10. The RMSEs of the retrieved atmospheric profiles for the actual IASI data in 2010. The dashed is the RMSEs before bias correction. The solid is the RMSEs after bias correction using the estimated biases from historical data of 2009. (a) For temperature profile; (b) for humidity profile.

Different from Fig. 6, there are obvious biases for both the atmospheric temperature and humidity profiles for actual IASI data. The biases for the temperature profiles changes from -5 K to 2 K. Meanwhile, the biases for the humidity profile are always negative within about -0.002 g/g. Those biases may be caused by several factors. The possible reasons are: 1) the remained forward errors in the radiative transfer model; 2) the unresolved errors in the sensor calibrations; and 3) the uncertainties about other trace gases when determining the regression coefficients, such as carbon monoxide or methane. These factors will make the proposed algorithm have the system bias errors, which implies that an on-orbit calibration for both measurements and forward RTM or a post calibration for atmospheric profiles may be required. Thanks to the availability of matchup data in 2009 for the same region, those system bias errors can be estimated directly from those historic data by comparing the differences between the estimated and actual atmospheric profiles. Consequently, those estimated biases were used to remove the system bias errors in 2010. The standard deviation of the retrieved atmospheric profiles for the actual IASI data is nearly

similar to, at most not more 1.5 times than that for the simulated IASI data.

Fig. 10 shows the RMSEs of the retrieved atmospheric profiles for the actual IASI data before and after correcting for bias errors. The RMSEs decrease along with the altitude for both temperature and humidity profiles. The maximum RMSEs before bias correction are about 6 K and 0.004 g/g for temperature and humidity profiles, respectively. However, the RMSEs can decrease to 2 K in troposphere and stratosphere and 3–5 K near the surface after bias correction. Although the retrieval accuracy for the actual IASI data is not as good as those for the simulated data, the proposed algorithm can be also thought as promising if the profile bias errors could be well removed.

V. Conclusions

In this work, a physics-based regression algorithm has been proposed to retrieve the atmospheric temperature and humidity profiles with three steps, including a selection of optimal channels, a principal component analysis, and a ridge regression procedure. Taking into account the difficulty of collecting the synchronous measurements, different combinations of ASTER Spectral Library and TIGR database were used to simulate various possible situations, and to determine the regression coefficients from the perturbation of brightness temperature to that of the atmospheric profiles.

To fully evaluate the proposed algorithm, both the simulated and actual IASI data were used to determine the accuracy of the proposed algorithm. The results with simulated data showed that the proposed algorithm is unbiased for various land surface and atmospheric conditions and be of robustness and speediness. The RMSEs of temperature profile are about 1.5 K in troposphere and stratosphere and close to 4 K near the surface. The worse accuracy near the surface may be caused by the couple of land-atmosphere and the selection channels. The RMSEs of humidity profile are about 0.001–0.003 g/g at low altitude and decreases greatly along with the altitude beyond the troposphere. Although the results with actual data are not as good as those for the simulated data, the vertical distribution of atmospheric profiles can be well captured. There are obvious biases for both the atmospheric temperature and humidity profiles, which may be resulted by the remained forward errors in the radiative transfer model, the unresolved errors in the sensor calibrations or the uncertainties about other trace gases. The standard deviation of the retrieved atmospheric profiles for the actual IASI data is not more 1.5 times than that for the simulated IASI data. Fortunately, these biases errors could be easily corrected through algorithm calibration. The RMSEs of temperature and humidity profile for the actual data become nearly the same as those for the simulated data after bias correction. The RMSEs of temperature profile decrease to 2 K in troposphere and stratosphere and 3–5 K near the surface.

In conclusion, the proposed algorithm is promising for the reasons of well characterization of vertical distribution of profiles and the possibility of removing biases. Nevertheless, more works should be done. How to quickly select more synchronous data to make the evaluation results become more confident, how to combine with the AMSU to well sound the near surface, and how to integrate with physical methods to improve the accuracies of retrieved atmospheric profiles will be studied in the near future.

Acknowledgment

The authors thank the anonymous referees for their comments and suggestions that have significantly improved the article. The authors would also like to sincerely thank NOVELTIS Inc. for providing the 4A/OP model, Jet Propulsion Laboratory for the ASTER spectral library, the Laboratoire de Meteorologie Dynamique for the TIGR database, the University of Wyoming for the radiosonde data, and the European Organization for the Exploitation of Meteorological Satellites for the IASI data.

References

[1] C. D. Rodgers, "Retrieval of atmospheric temperature and composition from remote measurements of thermal radiation," *Rev. Geophys.*, vol. 14, no. 4, pp. 609–624, 1976.

[2] X. L. Ma, Z. Wan, C. C. Moeller, W. P. Menzel, and L. E. Gumley, "Simultaneous retrieval of atmospheric profiles, land-surface temperature, and surface emissivity from Moderate-Resolution Imaging Spectroradiometer thermal infrared data: Extension of a two-step physical algorithm," *Appl. Optics*, vol. 41, no. 5, pp. 909–924, 2002.

[3] P. Dash, F. M. Gottsche, F. S. Olesen, and H. Fischer, "Land surface temperature and emissivity estimation from passive sensor data: Theory and practice-current trends," *Int. J. Remote Sens.*, vol. 23, no. 13, pp. 2563–2594, 2002.

[4] X. L. Ma, Z. Wan, C. C. Moeller, W. P. Menzel, L. E. Gumley, and Y. L. Zhang, "Retrieval of geophysical parameters from Moderate Resolution Imaging Spectroradiometer thermal infrared data: Evaluation of a two-step physical algorithm," *Appl. Optics*, vol. 39, no. 20, pp. 3537–3550, Jul. 2000.

[5] Z.-L. Li, B.-H. Tang, H. Wu, H. Z. Ren, G. J. Yan, Z. Wan, I. F. Trigo, and J. A. Sobrino, "Satellite-derived land surface temperature: Current status and perspectives," *Remote Sens. Environ.*, vol. 131, pp. 14–37, 2013.

[6] Z.-L. Li, H. Wu, N. Wang, S. Qiu, J. A. Sobrino, Z. Wan, B.-H. Tang, and G. J. Yan, "Land surface emissivity retrieval from satellite data," *Int. J. Remote Sens.*, vol. 34, no. 9–10, pp. 3084–3127, 2013.

[7] J. Li, E. Weisz, and D. K. Zhou, "Physical retrieval of surface emissivity spectrum from hyperspectral infrared radiances," *Geophys. Res. Lett.*, vol. 34, no. 16, p. L16812, 2007.

[8] N. Wang, Z.-L. Li, B.-H. Tang, F. N. Zeng, and C. R. Li, "Retrieval of atmospheric and land surface parameters from satellite-based thermal infrared hyperspectral data using a neural network technique," *Int. J. Remote Sens.*, vol. 34, no. 9–10, pp. 3485–3502, 2013.

[9] H. Wu and Z.-L. Li, "Scale issues in remote sensing: A review on analysis, processing and modeling," *Sensors*, vol. 9, no. 3, pp. 1768–1793, 2009.

[10] M. T. Chahine, H. Aumann, M. Goldberg, L. McMillin, P. Rosenkranz, D. Staelin, L. Strow, J. Susskind, and M. Gunson, "AIRS-team retrieval for core products and geophysical parameters," *AIRS Level 2 Algorithm Theoretical Basis Document Version 2.2, JPL D-17006*, vol. 2, 2001.

[11] W. L. Smith and H. M. Woolf, "The use of eigenvectors of statistical covariance matrices for interpreting satellite sounding radiometer observations," *J. Atmos. Sci.*, vol. 33, pp. 1127–1140, 1976.

[12] F. Aires, A. Chédin, N. A. Scott, and W. B. Rossow, "A regularized neural net approach for retrieval of atmospheric and surface temperatures with the IASI instrument," *J. Appl. Meteorol.*, vol. 41, pp. 144–159, 2002.

[13] F. Aires, W. B. Rossow, N. A. Scott, and A. Chédin, "Remote sensing from the infrared atmospheric sounding interferometer instrument, 2, Simultaneous retrieval of temperature, water vapor, and ozone atmospheric profiles," *J. Geophys. Res.*, vol. 107, no. D22, p. 4620, 2002.

[14] J. Li, F. Zhou, and Q. Zeng, "Simultaneous non-linear retrieval of atmospheric temperature and absorbing constituent profiles from satellite infrared sounder radiances," *Adv. Atmos. Sci.*, vol. 11, pp. 128–138, 1994.

[15] A. E. Hoerl and R. W. Kennard, "Ridge regression: Biased estimation for nonorthogonal problems," *Technometrics*, vol. 12, no. 1, pp. 55–67, 1970.

[16] A. D. Collard, "Selection of IASI channels for use in numerical weather prediction," *Quart. J. Roy. Meteor. Soc.*, vol. 133, no. 629, pp. 1977–1991, 2007.

[17] A. M. Baldridge, S. J. Hook, C. I. Grove, and G. Rivera, "The ASTER spectral library version 2.0," *Remote Sens. Environ.*, vol. 113, no. 4, pp. 711–715, 2009.
[18] J. M. Galve, C. Coll, V. Caselles, and E. Valor, "An atmospheric radiosounding database for generating land surface temperature algorithms," *IEEE Trans. Geosci. Remote Sens.*, vol. 46, no. 5, pp. 1547–1557, 2008.
[19] L. Chaumat, C. Standfuss, B. Tournier, R. Armante, and N. A. Scott, 4A/OP Reference Documentation NOVELTIS, LMD/CNRS, CNES, 2009, NOV-3049-NT-1178-v4.0.
[20] F. Aires, W. B. Rossow, N. A. Scott, and A. Chedin, "Remote sensing from the infrared atmospheric sounding interferometer instrument. 1. Compression, denoising, and first-guess retrieval algorithms," *J. Geophys. Res.*, vol. 107, no. D22, p. 4619, 2002.
[21] B.-H. Tang, Y. Y. Bi, Z.-L. Li, and J. Xia, "Generalized Split-Window algorithm for estimate of land surface temperature from Chinese geostationary FengYun meteorological satellite (FY-2C) data," *Sensors*, vol. 8, no. 2, pp. 933–951, 2008.

Hua Wu received the B.S. degree in photogrammetric engineering and remote sensing from Wuhan University, Wuhan, China, in 2003, the M.S. degree in cartography and geographical information system from Beijing Normal University, Beijing, China, in 2006, and the Ph.D. degree in cartography and geographical information system from the Institute of Geographic Sciences and Natural Resources Research, Chinese Academy of Sciences, Beijing, in 2010.

He is currently a Research Assistant with the Institute of Geographic Sciences and Natural Resources Research, Chinese Academy of Sciences. His research mainly includes the retrieval and validation of surface temperature and emissivities, and scaling of remotely sensed products.

Li Ni received the B.S. degree and the M.S. degree in photogrammetric engineering and remote sensing from Wuhan University, Wuhan, China, in 2003 and 2006, respectively. She is currently pursuing the Ph.D. degree in cartography and geographical information system at Center for Earth Observation and Digital Earth, Chinese Academy of Sciences.

She is currently a Research Assistant with the Center for Earth Observation and Digital Earth, Chinese Academy of Sciences. Her research interests focus on the hyperspectral remote sensing.

Ning Wang received the B.S. and M.S. in Geophysical Science and Cartography and Geographic Information System from the Beijing Normal University, China, in 2004 and 2007, respectively, and the Ph.D. degree in cartography and geographical information system from Institute of Geographic Sciences and Natural Resources Research, Chinese Academy of Sciences, Beijing, China in 2011.

He is currently a Research Assistant with the Academy of Opto-Electronics, Chinese Academy of Sciences. His research interests include thermal infrared remote sensing and hyperspectral remote sensing.

Yonggang Qian received the B.S. degree in applied mathematics from Yantai University, Yantai, China, in 2003, the M.S. degree in geographical information system from Taiyuan University of Technology, Taiyuan, China, in 2006, the Ph.D. degree in cartography and geographical information system from Beijing Normal University, Beijing, China, in 2009, and the Post Doctor in cartography and geographical information system from the Institute of Geographic Sciences and Natural Resources Research, Chinese Academy of Sciences, Beijing, in 2009–2011.

He is currently an Associate Research Fellow with the Academy of Opto-Electronics, Chinese Academy of Sciences. His research mainly includes the retrieval and validation of surface temperature and emissivity from remotely sensed data.

Bo-Hui Tang received the B.S. degree in cartography and geographical information system from Wuhan University, Wuhan, China, in 1999, the M.S. degree in cartography and geographical information system from China Remote Sensing Satellite Ground Station, Chinese Academy of Sciences, Beijing, China, in 2004, and the Ph.D. degree in cartography and geographical information system from the Institute of Geographic Sciences and Natural Resources Research, Chinese Academy of Sciences, Beijing, in 2007.

He is currently an Associate Research Fellow with the Institute of Geographic Sciences and Natural Resources Research, Chinese Academy of Sciences. His research mainly includes the retrieval and validation of surface net radiation and surface temperature.

Zhao-Liang Li received the Ph.D. degree in 1990. Since 1992, he has been a research scientist at CNRS, Illkirch, France. He joined the Institute of Agricultural Resources and Regional Planning in 2013. He has participated in many national and international projects such as NASA-funded MODIS, EC-funded program EAGLE, and ESA funded programs SPECTRA, etc. His main expertise fields are in thermal infrared radiometry, parameterization of land surface processes at large scale, as well as in the assimilation of satellite data to land surface models. He has published more than 100 papers in international refereed journals.